ENCIT 2018

ABCM Associação Brasileira de Engenharia e Ciências Mecânicas

17th Brazilian Congress of Thermal Sciences and Engineering
November 25th-28th, 2018, Águas de Lindóia, SP, Brazil

ENCIT-2018-0421
INFLUENCE OF THE STAGNATION PRESSURE RATIO ON THE ONSET OF RECIRCULATION ZONES IN INVISCID SUPERSONIC FLOWS

Marco Aurélio Leonel Matunaga
Instituto Tecnológico de Aeronáutica, DCTA/ITA, São José dos Campos, SP, Brazil
marco.matunaga@gmail.com

João Luiz F. Azevedo
Instituto de Aeronáutica e Espaço, DCTA/IAE/ALA, São José dos Campos, SP, Brazil
joaoluiz.azevedo@gmail.com

Luís Fernando Figueira da Silva
Pontifícia Universidade Católica do Rio de Janeiro, PUC-Rio, Rio de Janeiro, RJ, Brazil
luisfer@puc-rio.br

Abstract. *The present work is concerned with the study of the possibility of creating recirculation zones in inviscid supersonic flows. These regions can be useful, for instance, as flame holders in the case of supersonic combustion devices. The physical model adopted addresses the actual major interest of the present effort, which is to contribute towards the understanding of the origin of a recirculation bubble in an inviscid supersonic channel flow. The flows of interest here can be adequately modeled by the Euler equations in two dimensions. The solution of the system of governing equations is obtained using a total variation diminishing (TVD) method. The physical problem encompasses the analysis of the conditions in which the existence of a recirculation bubble is possible for inviscid supersonic flows. The results exhibit what are the flow and boundary condition combinations necessary to create recirculation bubbles in the flow.*

Keywords: *Computational Fluid Dynamics, Recirculation, Supersonic Flows*

1. INTRODUCTION

In the present work, the main interest is the study of the phenomenon of recirculation in inviscid supersonic flows. The problem of recirculation is important for some areas such as supersonic combustion. In these applications, the Mach number and the static temperature values inside the combustion chamber are critical for the ignition and the stabilization of combustion. Low values of these two parameters could preclude the self-ignition in the mixing layers and jets (Figueira da Silva *et al.*, 1997). To deal with this problem, many researchers have studied how to stabilize the combustion reaction using a recirculation zone (Winterfeld, 1968; Gruber *et al.*, 2004; Figueira da Silva *et al.*, 1997; Thakur and Segal, 2008; Mitani and Kouchi, 2005).

Several studies of free recirculation bubbles in supersonic non-reacting flows are available, such as those performed by Nedungadi and Lewis (1996); Smart and Kalkhoran (1995); Metwally *et al.* (1989); Mahesh (1996). In these studies, there is an interaction between a vortex and a shock wave, and the flow presents a total pressure deficit in a finite region. Typically, the region of reduced total pressure is a swirling flow region, where the vortex core presents an axial velocity deficit with respect to the outer region. In such studies, in order to create a recirculation zone, it is customary to change the relative intensities of the swirl and shock. These variations can cause a deformation of the shock wave and, in some cases, the bulging can create a stagnation region.

Studies on the effect of the shock strength, *i.e.*, the influence of the shock angle on the onset of a recirculation can be found in Smart and Kalkhoran (1995); Metwally *et al.* (1989); Kalkhoran *et al.* (1996); Kalkhoran (1994); Cattafesta III and Settles (2001). Basically, for larger shock wave angles, the pressure gradients are sufficiently strong to create a subsonic flow downstream the shock wave, which then stagnates the flow eventually. Such recirculation region is not solely created by the interaction between the shock wave and the vortex, or a region with swirling flow. Indeed, Klass *et al.* (2002) show that an important factor to start the recirculation zone is the vortex axial velocity deficit. Similarly, Rizetta (1997) and Nedungadi and Lewis (1996) argue that the axial velocity deficit plays a significant role on the recirculation zone formation.

The present work studies the onset mechanisms of 2-D recirculation bubbles in inviscid supersonic flows. The evaluated geometry is a channel, *i.e.*, the top and bottom boundaries are infinite plates and the flow passes between these two

structures. The beginning of the recirculation is assessed as a function of stagnation pressure deficit in a finite flow region. The main objective of this paper is to provide an overview of resulting flow topology of a 2-D recirculation zone in a channel. The main contribution of the present work is the analysis of the recirculation phenomenon solving the 2-D Euler equations.

In the present paper, the Harten method (Harten, 1983) has been used to obtain the numerical solutions for the 2-D Euler equations. An explicit version of this numerical method is implemented in a Fortran90 code. In order to validate the computational tool, shock wave reflection problems are solved as test cases and compared to the analytical solution. Since such test case has two well-defined discontinuities, this problem is ideal to demonstrate the method shock-capturing capabilities. The paper structure is divided as follows, Sect. 2, presents the Harten method, Sect. 3 presents the geometry used in the numerical simulations, Sect. 4 shows the numerical solutions and Sect. 5 presents the conclusions of the present work.

2. NUMERICAL METHODOLOGY

The numerical scheme, which is commonly referred to as the Harten method, or Harten's TVD method, was presented in Harten (1983). This method was initially developed for non-stationary problems (Harten, 1983, 1984). The Harten method belongs to a special class of numerical methods, known as total variation diminishing (TVD) schemes. Harten's TVD method is constructed to be monotonicity preserving, 2nd-order accurate both in time and in space (Harten, 1983). The numerical scheme implements a nonlinear limiter, which allows the 2nd-order method to adequately capture strong shock waves. Near discontinuous regions, the method is 1st-order accurate due to the limiter. Furthermore, the method enforces an entropy condition (Toro, 1997; Versteeg and Malalasekera, 2007), such that the scheme only converges to physically relevant solutions (LeVeque, 2002).

2.1 Harten Scheme Applied to the Euler Equations

The physical problem addressed in the present study allows the use of a 2-D inviscid formulation. The Euler equations in two dimensions are given by

$$\frac{\partial Q}{\partial t} + \frac{\partial F(Q)}{\partial x} + \frac{\partial G(Q)}{\partial y} = 0\,, \tag{1}$$

where

$$Q = \begin{bmatrix} \rho \\ \rho u \\ \rho v \\ E \end{bmatrix}\,, \qquad F = \begin{bmatrix} \rho u \\ \rho u^2 + p \\ \rho uv \\ u(E+p) \end{bmatrix}\,, \qquad G = \begin{bmatrix} \rho v \\ \rho uv \\ \rho v^2 + p \\ v(E+p) \end{bmatrix}\,, \tag{2}$$

where the variables are density, which is denoted by ρ, velocity components in the x-direction and in the y-direction, u and v, pressure, p, and E represents the total energy per unit of volume, which is related to the pressure p by the equation of state. In the present work, since an ideal gas is assumed, this relation can be written as

$$p = (\gamma - 1)\left[E - \frac{\rho(u^2 + v^2)}{2}\right]. \tag{3}$$

The numerical solutions are obtained through the following expression

$$Q^{n+1}_{j,k} = Q^n_{j,k} - \frac{\Delta t}{\Delta x}\left(\tilde{F}^n_{j+1/2,k} - \tilde{F}^n_{j-1/2,k}\right) - \frac{\Delta t}{\Delta y}\left(\tilde{G}^n_{j,k+1/2} - \tilde{G}^n_{j,k-1/2}\right). \tag{4}$$

The mesh spacing in the x-direction and in the y-direction are denoted by Δx and Δy, respectively. The index j and the index k refer to the x-direction and to the y-direction, respectively. The numerical fluxes for the 2-D second order Harten method are defined as

$$\tilde{F}^n_{j+1/2,k} = \frac{1}{2}\left[F_j + F_{j+1} + \frac{\Delta x}{\Delta t}\sum_{m=1}^{4}\left(g^m_j + g^m_{j+1} - \psi^m\left(\nu_{j+1/2} + \gamma_{j+1/2}\right)\alpha^m_{j+1/2}\right)R^m_{j+1/2}\right] \tag{5}$$

and

$$\tilde{G}^n_{j,k+1/2} = \frac{1}{2}\left[G_k + G_{k+1} + \frac{\Delta y}{\Delta t}\sum_{m=1}^{4}\left(g^m_k + g^m_{k+1} - \psi^m\left(\nu_{k+1/2} + \gamma_{k+1/2}\right)\alpha^m_{k+1/2}\right)R^m_{k+1/2}\right]. \tag{6}$$

In order to determine the values of $Q_{j+1/2,k}$ and $Q_{j,k+1/2}$ the Roe's averaging process is used (Roe, 1981), *i.e.*,

$$u_{j+1/2} = \frac{\sqrt{\rho_j}u_j + \sqrt{\rho_{j+1}}u_{j+1}}{\sqrt{\rho_j} + \sqrt{\rho_{j+1}}}, \tag{7}$$

$$H = \frac{(E+p)}{\rho}, \tag{8}$$

$$H_{j+1/2} = \frac{\sqrt{\rho_j}H_j + \sqrt{\rho_{j+1}}H_{j+1}}{\sqrt{\rho_j} + \sqrt{\rho_{j+1}}}, \tag{9}$$

$$c_{j+1/2} = \left[(\gamma-1)\left(H_{j+1/2} - 0.5\left\{u^2_{j+1/2} + v^2_{j+1/2}\right\}\right)\right]. \tag{10}$$

2.2 The Additional g Flux

In Eqs. (5) and (6),the term denoted by g, is expressed as

$$g^m_j = sign(\tilde{g}^m_{j+1/2}) \;\; \max\left[0, \min\left(|\tilde{g}^m_{j+1/2}|, \tilde{g}^m_{j-1/2} \;\; sign(\tilde{g}^m_{j+1/2})\right)\right]. \tag{11}$$

In order to calculate the numerical fluxes, Eq. (5), Eq. (6) and the new flux g, defined in Eq. (11), it is necessary to define the function $\tilde{g}$ term, which is given by

$$\tilde{g}^m_{j+1/2} = \frac{1}{2}\left[\psi^m\left(\nu^m_{j+1/2}\right) - \left(\nu^m_{j+1/2}\right)^2\right]\alpha^m_{j+1/2}. \tag{12}$$

The flow studied presents discontinuities, such as shock waves, which are characterized by discontinuous property changes, which can degrade the numerical solution. To avoid this, it is necessary to introduce a procedure to control the numerical oscillations caused by these discontinuities. The function g, which is defined in Eq. (11), is formulated to deal with the numerical oscillations. Its definition presents a nonlinear term, known as the *minmod* limiter (Roe, 1986; LeVeque, 2002). This nonlinear term prevents new maximum and minimum values in the numerical solution and it enforces the TVD property (Harten, 1983).

Yee *et al.* (1982) and Yee *et al.* (1985) show two different methods to calculate the ν function. For the present study, the value of ν is given by

$$\nu^1_{j+1/2} = \frac{\Delta t}{\Delta x}a^1_x = \frac{\Delta t}{\Delta x}(\hat{u} - \hat{c}), \tag{13}$$

$$\nu^2_{j+1/2} = \frac{\Delta t}{\Delta x}a^2_x = \frac{\Delta t}{\Delta x}(\hat{u}), \tag{14}$$

$$\nu^3_{j+1/2} = \frac{\Delta t}{\Delta x}a^3_x = \frac{\Delta t}{\Delta x}(\hat{u} + \hat{c}), \tag{15}$$

$$\nu^4_{j+1/2} = \frac{\Delta t}{\Delta x}a^4_x = \frac{\Delta t}{\Delta x}(\hat{u}). \tag{16}$$

The numerical fluxes encompasses the eigenvalues and eigenvectors obtained from the fluxes of the hyperbolic conservation laws. To apply the Harten method to the Euler equations, one rewrites the Eq. (1) as

$$\frac{\partial Q}{\partial t} + A\frac{\partial Q}{\partial x} + B\frac{\partial Q}{\partial y} = 0, \tag{17}$$

where A is the Jacobian matrix, given by $A = \partial F(Q)/\partial Q$, whose eigenvalues are

$$(\lambda^1_x, \lambda^2_x, \lambda^3_x, \lambda^4_x) = (u - c, u, u + c, u), \tag{18}$$

where, c is the local speed of sound. The right eigenvectors of the A matrix form the matrix $R_x = (R^1_x, R^2_x, R^3_x, R^4_x)$, where

$$R_x = \begin{bmatrix} 1 & 1 & 1 & 0 \\ u-c & u & u+c & 0 \\ v & v & v & 1 \\ H-uc & (u^2+v^2)/2 & H+uc & v \end{bmatrix}_{j+1/2}. \tag{19}$$

Here, H is the total enthalpy, given by

$$H = \frac{c^2}{\gamma - 1} + \frac{u^2 + v^2}{2}. \tag{20}$$

Therefore, one can be define the vector $\alpha = \Delta w = R^{-1}\Delta Q$ in the x-direction. To simplify the notation, only the x-direction index j will be shown. The α vector is given by

$$\begin{bmatrix} \alpha^1_{j+1/2} \\ \alpha^2_{j+1/2} \\ \alpha^3_{j+1/2} \\ \alpha^4_{j+1/2} \end{bmatrix} = \begin{bmatrix} (aa - bb)/2 \\ \Delta_{j+1/2}\rho - aa \\ (aa + bb)/2 \\ \Delta_{j+1/2}\rho v - v_{j+1/2}\Delta_{j+1/2}\rho \end{bmatrix}, \tag{21}$$

where

$$\Delta_{j+1/2}\left(\right) = \left(\right)_{j+1} - \left(\right)_j, \tag{22}$$

$$aa = \frac{\gamma - 1}{c^2_{j+1/2}} \left[\Delta_{j+1/2}e + \frac{u^2_{j+1/2} + v^2_{j+1/2}}{2}\Delta_{j+1/2}\rho - u_{j+1/2}\Delta_{j+1/2}\rho u - v_{j+1/2}\Delta_{j+1/2}\rho v \right], \tag{23}$$

and

$$bb = \frac{\left[\Delta_{j+1/2}\rho u - u_{j+1/2}\Delta_{j+1/2}\rho\right]}{c_{j+1/2}}. \tag{24}$$

For the y-direction the Jacobian matrix is denoted by B, which is given by $B = \partial G(Q)/\partial Q$, whose eigenvalues are

$$(\lambda^1_y, \lambda^2_y, \lambda^3_y, \lambda^4_y) = (v - c, v, v + c, v). \tag{25}$$

The right eigenvectors of B form the matrix $R_y = (R^1_y, R^2_y, R^3_y, R^4_y)$, as

$$R_y = \begin{bmatrix} 1 & 1 & 1 & 0 \\ u & u & u & 1 \\ v - c & v & v + c & 0 \\ H - vc & (u^2 + v^2)/2 & H + vc & u \end{bmatrix}_{k+1/2}. \tag{26}$$

The vector α in the y-direction is defined as

$$\begin{bmatrix} \alpha^1_{k+1/2} \\ \alpha^2_{k+1/2} \\ \alpha^3_{k+1/2} \\ \alpha^4_{k+1/2} \end{bmatrix} = \begin{bmatrix} (cc - dd)/2 \\ \Delta_{k+1/2}\rho - cc \\ (cc + dd)/2 \\ \Delta_{k+1/2}\rho u - u_{k+1/2}\Delta_{k+1/2}\rho \end{bmatrix}, \tag{27}$$

where index j is omitted for simplicity. The values of cc and dd are given by

$$cc = \frac{\gamma - 1}{c^2_{k+1/2}} \left[\Delta_{k+1/2}E + \frac{u^2_{k+1/2} + v^2_{k+1/2}}{2}\Delta_{k+1/2}\rho - u_{k+1/2}\Delta_{k+1/2}\rho u - v_{k+1/2}\Delta_{k+1/2}\rho v \right], \tag{28}$$

and

$$dd = \frac{\left[\Delta_{k+1/2}\rho v - v_{k+1/2}\Delta_{k+1/2}\rho\right]}{c_{k+1/2}}. \tag{29}$$

2.3 Functions ψ and γ

The Harten method obeys an entropy jump inequality. Therefore, the numerical scheme only converges to physically relevant solutions (Harten, 1983). This ψ function is formulated in order to satisfy the entropy jump inequality (Harten, 1983). Moreover, this function adds a small amount of artificial viscosity in the numerical solution. The ψ and γ functions are given by

$$\psi^m(z) = \begin{cases} \dfrac{1}{2}\left(\dfrac{z^2}{\epsilon^m} + \epsilon^m\right), & |z| < \epsilon^m \\ |z|, & |z| \geqslant \epsilon^m \end{cases}, \tag{30}$$

and

$$\gamma^m_{j+1/2} = \begin{cases} \dfrac{\left(g^m_{j+1} - g^m_j\right)}{\alpha^m_{j+1/2}}, & \alpha^k_{j+1/2} \neq 0 \\ 0, & \alpha^m_{j+1/2} = 0 \end{cases}. \tag{31}$$

The ϵ parameter directly influences the method performance. According to Harten (1983), for larger values of ϵ, the method presents an improvement in entropy enforcement, *i.e.*, the numerical solutions can converge to the unique physical solution of conservation laws. The ϵ values are given by

$$\epsilon^m = 0.01 \;\; if \;\; \frac{\partial \lambda^m}{\partial Q} R^m \neq 0 \tag{32}$$

$$\epsilon^m = 0.0 \;\; if \;\; \frac{\partial \lambda^m}{\partial Q} R^m \equiv 0 \tag{33}$$

One problem of using larger values of ϵ, such as 0.2 is the loss in the resolution. Therefore, the values used for the problems are $\epsilon = 0.01$ for genuinely nonlinear fields and 0 for linearly degenerate fields, given by Eq. (32) and (33), respectively.

3. PROBLEM DEFINITION, INITIAL AND BOUNDARY CONDITIONS

The model used to assess the recirculation bubble onset phenomenom is described in this section. The main idea is to emulate a region of lower stagnation pressure as indicated in Figueira da Silva *et al.* (1997) and Nedungadi and Lewis (1996). These studies have shown that the region of lower stagnation pressure is an important factor in the onset of recirculation regions.

3.1 Computational Domain

The main interest of the present paper is to obtain the conditions under which a recirculation bubble may appear in a supersonic flow. In order to evaluate the onset of this recirculation zone the parameters chosen are the stagnation pressure deficit, the Mach number and the shock wave strength. A stationary recirculation bubble could be used to stabilize a supersonic combustion zone at lower supersonic Mach numbers (Nedungadi and Lewis, 1996; Winterfeld, 1968; Figueira da Silva *et al.*, 1997).

In order to understand the problem setup, it is convenient to discuss the details in two steps. Consider the flow illustrated in Fig. 1, *i.e.*, the two incoming streams of region 1 and 2 are assumed to be parallel at the entrance of the computational domain. Region 2 is a zone of undisturbed flow, whereas flow properties at region 3 are determined as if the flow went through an oblique shock wave, as indicated in Fig. 1, which would form an angle β with respect to the original flow direction. It is important to emphasize that this β angle is used to compute the shock jump conditions in region 3, only.

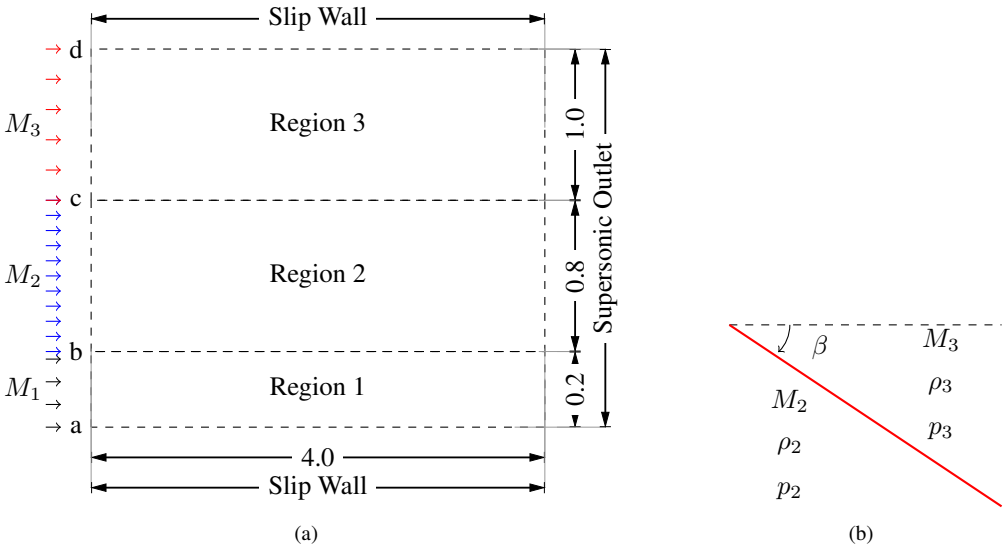

Figure 1. Flow initial topology for the recirculation bubble onset problem.

The boundary conditions described in Fig. 1 lead to the flow structures shown in Fig. 2. This illustration presents the numerical results for $M_1 = M_2$. The main flow structures expansion fans and shock waves. However, in order to

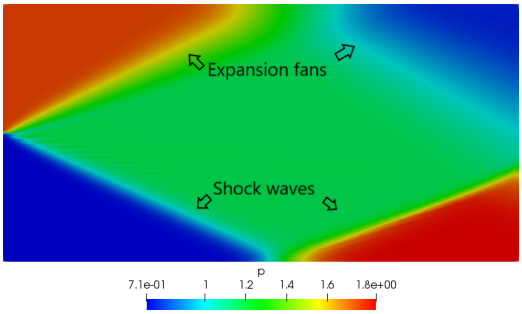

Figure 2. Description of the main flow features observed without recirculation.

trigger the possible creation of the recirculation bubble, a region with a momentum deficit should be created near the lower boundary of the computational domain. Hence, in order to study the recirculation bubble problem in a supersonic flow, the Mach number of region 1 is decreased, see Fig. 1. To accomplish this, the inlet boundary is divided into segments a-b (0.2 dimensionless length units), b-c (0.8 dimensionless length units) and c-d (1.0 dimensionless length units), respectively linked to regions 1, 2 and 3, as shown in Fig. 1. Moreover, the computational domain has two slip walls as indicated in Fig. 1(a). Region 1 has a lower stagnation pressure in relation to region 2, following Figueira da Silva *et al.* (1997) and Nedungadi and Lewis (1996). In order to obtain this lower stagnation pressure at region 1, the Mach number is smaller in region 1. In inlet regions 1 and 2, the static pressure and the density are the same, and they are imposed since as the flow supersonic at the entrance. Flow conditions at region 3 are determined as previously described. Therefore, the static pressure and the density in region 3 are larger than their corresponding values in region 2, and the velocity component in the x-direction is lower than the value of region 2. A detailed explanation about the equations used in the initial and boundary conditions is deferred to Sects. 3.2and 3.3

In the present work, all flow properties are non-dimensional values, the * superscript indicates dimensionless flow properties. The velocity component in the x-direction, u, is non-dimensionalized by the flow conditions at region 2 as

$$u^* = \frac{u}{c_2}\,, \tag{34}$$

where *c* and *M* are, respectively, the speed of sound and the Mach number. The subscript 2 denotes properties in region 2. The pressure is non-dimensionalized as

$$p^* = \frac{p}{\rho_2 c_2^2} = \frac{p}{\rho_2\left(\dfrac{\gamma p_2}{\rho_2}\right)} = \frac{p}{\gamma p_2}, \tag{35}$$

where γ is the ratio of specific heats and, in this case, $\gamma = 1.4$. The density is non-dimensionalized as

$$\rho^* = \frac{\rho}{\rho_2}, \tag{36}$$

where ρ_2 is the density at region 2.

3.2 Initial Conditions

First, to initialize this problem, the region 1 has the same flow properties values from region 2. The flow properties in those two regions are determined considering Eqs. (34) to (36). Therefore the flow initial conditions are

$$u^* = \frac{u_2}{c_2} = M_2, \tag{37}$$

$$p^* = \frac{p_2}{\rho_2 c_2^2} = \frac{p_2}{\rho_2\left(\dfrac{\gamma p_2}{\rho_2}\right)} = \frac{1}{\gamma}, \tag{38}$$

$$\rho^* = \frac{\rho_2}{\rho_2} = 1. \tag{39}$$

The flow conditions at region 3 of Fig. 1 are determined considering post shock conditions, where the upstream conditions are the properties values from Eqs. (37) to (39).

3.3 Boundary Conditions

The four boundary conditions, which are indicated in Fig. 1, have non-dimensional flow properties. Table 1 presents the flow properties values for all boundaries. The inlet boundary is divided into three regions, as shown in Fig. 1. The flow properties for region 3 are determined by the oblique shock wave relations. In order to that, one has to consider the flow conditions upstream the shock wave as the flow conditions at region 2. Therefore, region 3 corresponds to the flow conditions downstream of a shock wave, Fig. 1(b) illustrates this procedure. In region 2, the two velocity components are determined by

$$u^* = M_2\, c_2, \tag{40}$$

$$v^* = v = 0. \tag{41}$$

In region 1, a smaller stagnation pressure is imposed with respect to that of region 2. In order to achieve that, the Mach number in region 1 is obtained through the relation between the stagnation pressure from region 1 to region 2,

$$(p_0)_1 = (r)\,(p_0)_2\,. \tag{42}$$

When the equation for the stagnation pressure is substituted into Eq. (42), and after some mathematical manipulation, the Mach number in region 1 is obtained as

$$M_1 = \sqrt{\frac{2\,(A-1)}{\gamma-1}}; \qquad A = (r)^{\dfrac{\gamma-1}{\gamma}\left[1+\dfrac{(\gamma-1)}{2}M_2^2\right]}, \tag{43}$$

where r is the stagnation pressure ratio. Therefore, r is clearly related to the entropy change, *i.e.*, the entropy increase between regions 1 and 2. Therefore, by the Crocco-Vazsonyi equation Kundu *et al.* (2015), the vorticity vector is different from zero.

The computational domain has three other boundaries: one supersonic outlet and two slip walls, see Fig. 1. The conserved flow properties are extrapolated at these boundaries. Moreover, for the slip walls, the velocity component in the y-direction is equal to zero. The two last columns of Table 1 show how to prescribe these boundaries. The indexes $imax$ and $jmax$ correspond to the maximum number of points in the x and y-directions, respectively.

Table 1. Boundary conditions for the recirculation cases.

Variables	**Inlet Boundary**			**Supersonic Outlet**	**Slip Walls**
	Region 1	**Region 2**	**Region 3**		
ρ^*	1	1	Oblique Shock Wave Relations	$Q_{imax,j} = Q_{imax-1,j}$	$Q_{i,1} = Q_{i,2}$ $Q_{i,jmax} = Q_{i,jmax}$ v = 0
p^*	$1/\gamma$	$1/\gamma$			
u^*	Eq. (43)	Eq. (40)			
v^*	0	0	0		

4. RESULTS AND DISCUSSION

The results for the recirculation problem in inviscid supersonic flows are presented in this section. The Harten method has been implemented in a Fortran90 code and validated by solving the 2-D Euler equations for the shock wave reflection problem. The details of this validation process can be found in Matunaga (2018). The main objective of this section is to analyze the flowfield for the onset of recirculation zones. The relevant flow parameters are the β angle, which is shown in Fig. 1, the stagnation pressure and the Mach number at the inlet boundary in region 2. The problem studied is a non-stationary one, therefore it is not plausible to analyze the residue history from the numerical simulations.

4.1 Case Setup

In the present paper, two case solutions are presented. These cases are chosen because they presented the most complex flow structures observed. Both are obtained at 14 dimensionless time units after the initialization of the simulation, where the time step is constant and equal to 1.4×10^{-4} dimensionless time units. The mesh used in all cases is uniformly spaced and has 550 points in the x-direction and 320 points in the y-direction. This mesh setup has been chosen because considering the results obtained for the shock capturing property, see Matunaga (2018) for the details about the mesh evaluation. Moreover, these two cases have $M_2 = 3$ in region 2, and a β angle equals to 50 deg. The only difference is the stagnation pressure deficit, which is denoted by r. For the first case, this parameter is equals to 10% and, for the second case, the stagnation pressure deficit is increased to 20%. All solutions presented in the present paper are non-stationary and only the snapshot of the solution at the final time is given.

4.2 Case 1: Stagnation Pressure Ratio 10% $(SPR10)$

The flowfield for the first case with recirculation is presented in Fig. 3. In region 2, the Mach number is equal to 3,

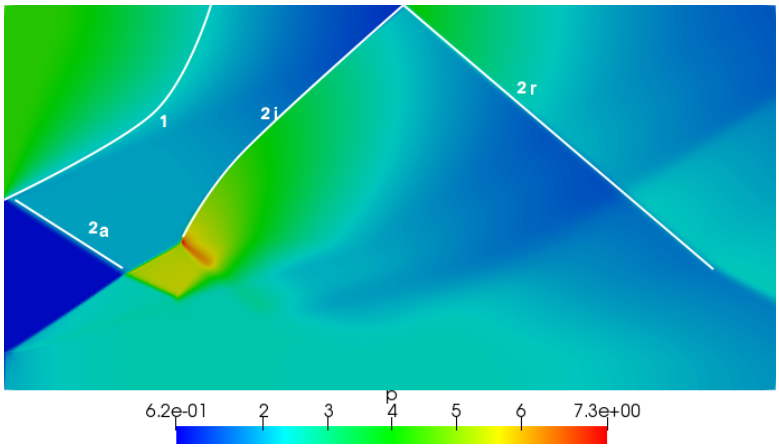

(a) Pressure contours. 1: expansion fan, 2a: shock wave stemming from the boundary conditions, 2i: incident shock wave and 2r: reflected shock wave.

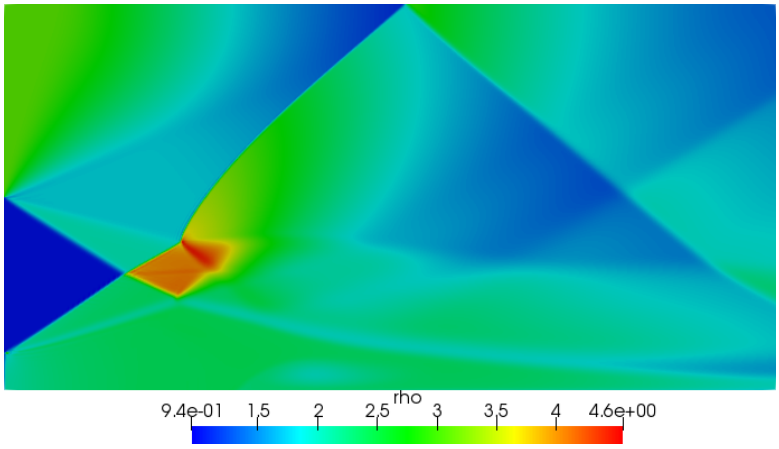

(b) Density contours.

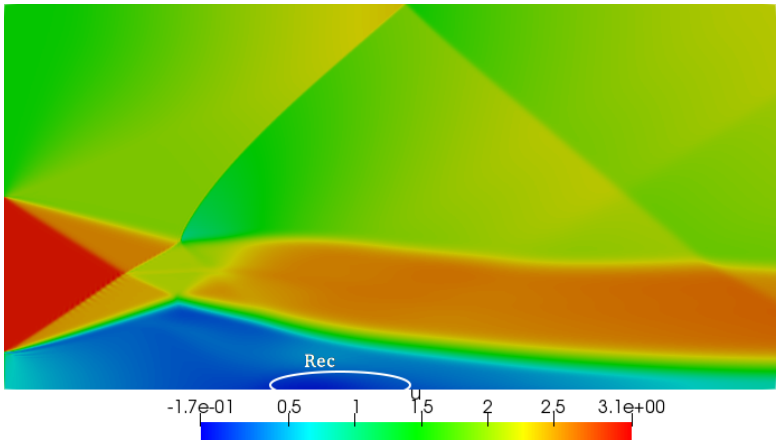

(c) Contours for the velocity component in the x-direction. Rec: recirculation region.

Figure 3. Flow property contours for case $SPR10$ using a 550×320 points mesh.

the stagnation pressure deficit is equal to 10% and the β angle is equal to 50 deg. These three values are the inputs for the present case, whereas the values obtained for the regions at the inlet are shown in Table 2. In Fig. 3, the main features of the flow are indicated by numbers. Indeed, number 1 indicates an expansion fan and number 2 indicates shock waves. The imposed boundary conditions of region 3 create an expansion fan near the inlet boundary, as indicated by the number 1 in Fig. 3. This flow structure avoid an unsteady shock at the lower region, however an unsteady shock is likely to occur

Table 2. Values computed for the inlet boundary.

Variables	**Region**		
	Region 1	**Region 2**	**Region 3**
ρ	1	1	3.08
p	0.71	0.71	4.28
u	1.5	3	1.48
v	0	0	0

at larger pressure ratios between regions 3 and 2. Moreover, Fig. 3 shows the shock wave at the entrance indicated by 2a in the same figure. This shock wave does not reaches the bottom boundary because of the recirculation zone, which is onset by low values of stagnation pressure of region 1. Another shock wave emerges in the flow, which is indicated by label 2i. This discontinuity reaches the upper boundary creating a new shock wave, indicated by tag 2r. In this case, there is a recirculation zone in the lower boundary, this region is represented in Fig. 3(c) by the word "Rec". It is important to emphasize that this recirculation zone is unsteady, *i.e.*, it moves towards the inlet boundary. Notice that all results are non-stationary and the figures represent the snapshot of the solution at 14 dimensionless units of time.

4.3 Case 2: Stagnation Pressure Ratio 20% $(SPR20)$

In relation to the previous case, the only change is the stagnation pressure ratio , *i.e.*, the r parameter. For the present case, this parameter is increased to 20%. The flow properties has the same values of the previous case, which are shown in Table 2. The Mach number in region 1 is the only exception, because it is calculated as a function of the r parameter, see Eq. (43). The resulting flowfield presents similar flow structures, *i.e.*, three shock waves and a recirculation zone, as may seen in Figure 4 Similarly to the previous case, the shock wave reflection phenomena, expansion fan and recirculation zone are present. However, some differences are visible. The first one is that pressure values downstream of the incident shock wave are lower than at the corresponding region for case 1. Indeed, the entire pressure field has lower pressure values of pressure than in the previous case. Again, cases 1 and 2 are nonstationary test cases and Figs. 3 and 4 represent the solution at 14 dimensionless time unit. The recirculation region for the present case presents the same movement of the previous one, *i.e.*, it moves towards the inlet boundary. Its final position, after 14 dimensionless time units, is closer to the inlet boundary than in the first case. Therefore, the recirculation zone for this case moves faster than in the previous one.

4.4 Recirculation Zone Comparison

In Figs. 3 and 4, the negative values of the velocity component in the x-direction indicates that there is indeed a recirculation zone. In order to analyze the internal recirculation zone pattern, particle paths for both cases are plotted and analyzed. Figure 5 presents a zoom of the recirculation zone for the two cases. Moreover, the Eulerian particle paths are shown for the same longitudinal extension of the flow are also given. The figure shows that the recirculation zone in case 1 is around 50% smaller than that of case 2. Furthermore, for the second case, the recirculation zone pattern is more complex. It is not just one recirculation zone as in the first case, three small regions of recirculation as shown in Fig. 5(b) are found to occur.

4.5 Influence of β and M_2

The influence of other flow parameters, β and M_2, is also evaluated. In the present work, a minimum value of stagnation pressure ratio, denoted by r, is determined for those two parameters. In order to assess the influence of β and M_2, numerical simulations are made in a 100×100 mesh. It is a coarser mesh than that used in the previous computations, because several numerical simulations are required to evaluate the onset of the recirculation zone. Therefore, using a coarser mesh means less computational costs, *i.e.*, saving CPU time. Moreover, the objective of the present work is to understand the main features of the flow instead of determine a value or range of values for the stagnation pressure ratio deficit where the recirculation starts. Therefore, the results of the present section provide data about the influence of each flow parameter on the onset of recirculation zones.

The stagnation pressure ratio parameter is defined in Eq. (43). This parameter is used to assess when a recirculation zone starts for specific values of β and M_2. Figure 6 shows the threshold values for the r parameter in which there is a recirculation zone. Above these values, no recirculation has been observed. From the plot in Fig. 6, as the β angle increases, the value for r necessary to obtain a recirculation zone is larger, *i.e.*, for a larger β the range of flows, in which there is a recirculation, is wider. Considering the shock wave indicated by 2a in Figs. 3 and 4, when the β angle is incremented, the pressure downstream the shock wave 2a is also increased, *i.e.*, the flow presents stronger shocks. Hence,

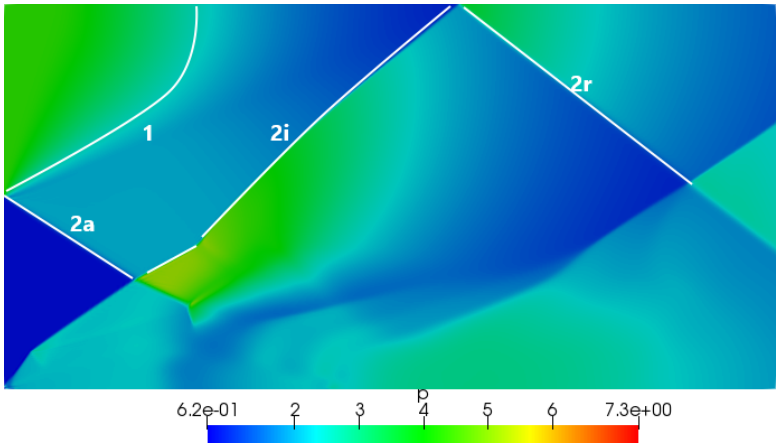

(a) Pressure contours. 1: expansion fan, 2a: shock wave created from the boundary conditions, 2i: incident shock wave and 2r: reflected shock wave.

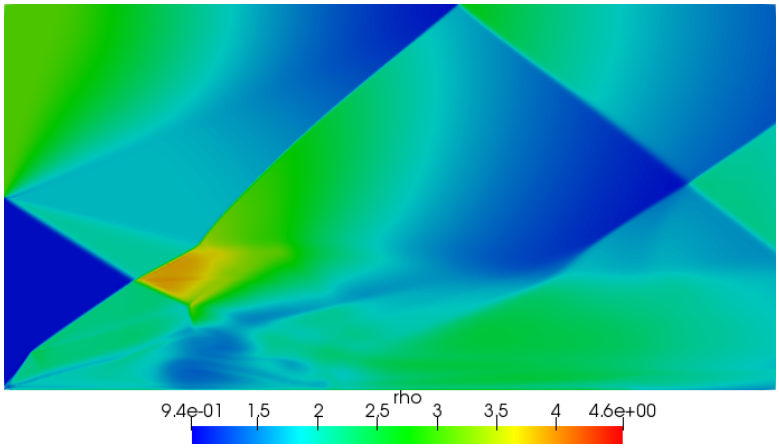

(b) Density contours.

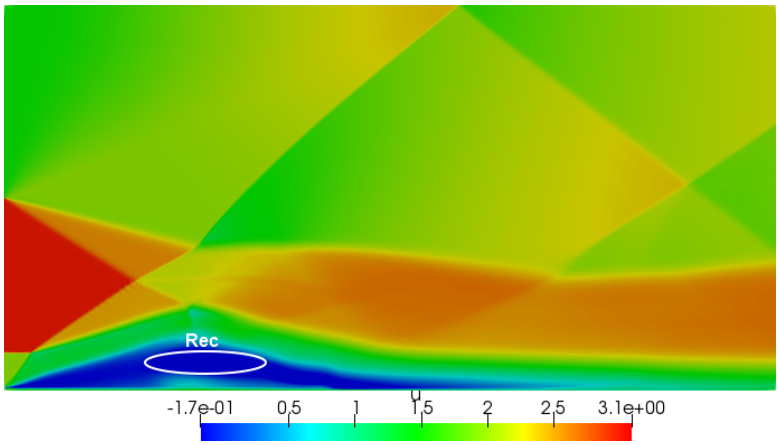

(c) Contours for the velocity component in the x-direction. Rec: recirculation region.

Figure 4. Flow property contours for case $SPR20$ using a 550×320 point mesh.

more entropy should be introduced in the flow, which by the Crocco-Vazsonyi equation means introducing vorticity in the flow (Kundu *et al.*, 2015). Therefore, increasing the β parameter involves higher likelihood of obtaining a recirculation zone. When the flow Mach number in region 2 is increased, it is necessary to decrease the stagnation pressure on region 1 in order to observe a recirculation zone. Increasing the flow Mach number, M_2, leads to higher flow velocities. Therefore, it is necessary to decrease the stagnation pressure ratio, r, in order to stagnate the flow.

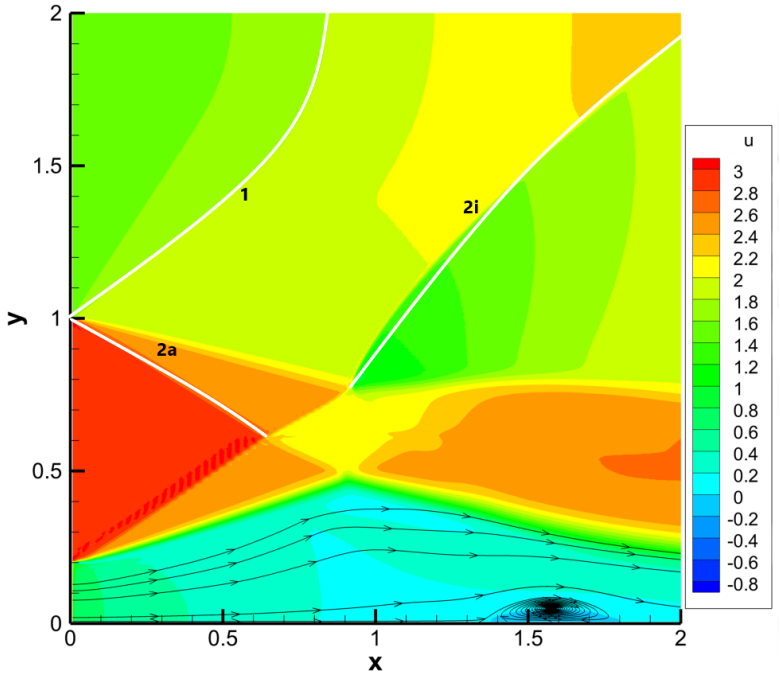

(a) RecZone 1 recirculation zone.

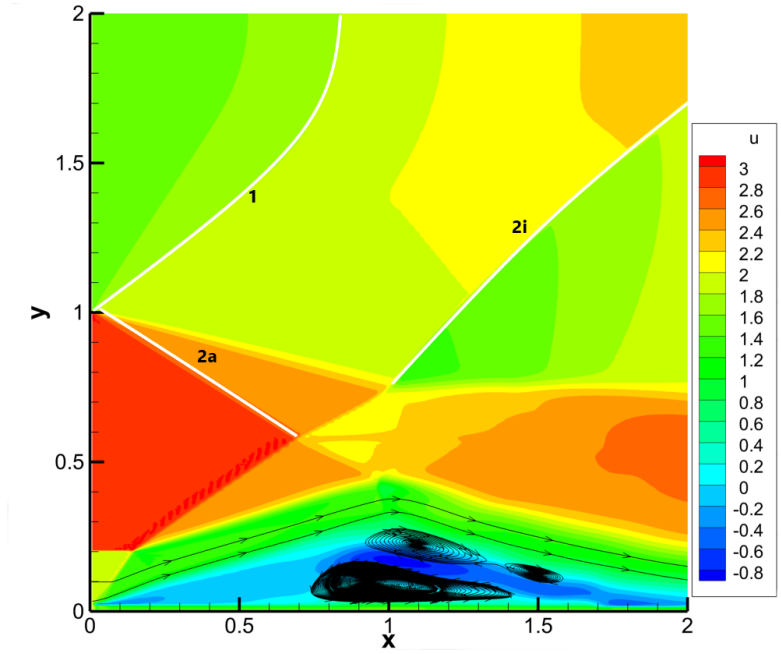

(b) RecZone 2 recirculation zone.

Figure 5. Comparison between the recirculation zones. 1: expansion fan, 2a: shock wave created from the boundary conditions and 2i: incident shock wave.

5. CONCLUDING REMARKS

The present work has addressed the formation of recirculation bubbles in supersonic inviscid flows. A flow configuration has been set up such that it attempts to emulate previous work in the literature, by creating a system of shock waves and expansion regions, and a total pressure deficit closer to the lower wall. The main idea is to emulate the flow with a region of lower stagnation pressure that has been reported in experiments with shock-vortex interactions. Moreover, this pattern helps to demonstrate the influence of the flow properties on the onset of the recirculation zone. In the present paper, the effects of the stagnation pressure deficit are evaluated.

The present results have been able to identify conditions under which recirculation zones can appear in planar two-dimensional (2-D) inviscid supersonic flows. The conditions for the onset of these recirculation bubbles have some

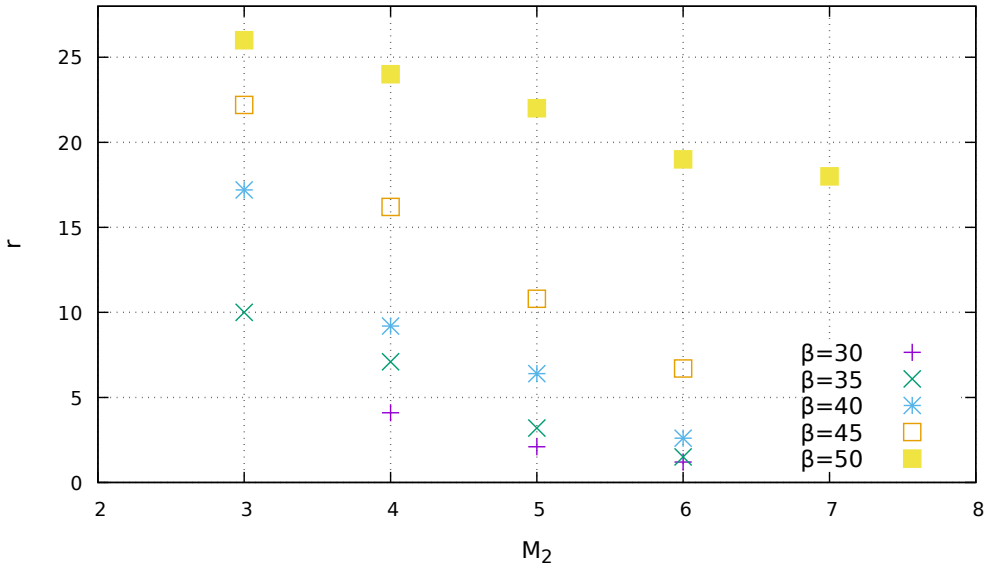

Figure 6. Threshold values of the *r* parameter required to obtain a recirculation zone evaluated for different values of β and M_2. Above these values no recirculation zone is observed.

resemblance with those previously observed in the literature for three-dimensional or axisymmetric flows. However, for the range of flow parameter here investigated, it was not possible to identify conditions under which a stable recirculation zone is formed in 2-D inviscid supersonic flows. In the present study the viscosity is neglected, therefore the vorticity created by viscosity is disconsidered. However, the work has demonstrated that a region with lower stagnation pressure can originate a recirculation zone in inviscid supersonic flows. Moreover, the present study provides details about the mechanisms of the onset of recirculation zones in inviscid supersonic flows. The main parameter considered is the stagnation pressure, a parameter that provides a relation between vorticity and entropy. The influences of Mach number and a novel parameter, β angle, on the onset of recirculation zones are also evaluated. This study analyzed these parameters influence on the stagnation pressure ratio necessary to obtain a recirculation zone. For the β angle, it was shown that as its value is increased, it is possible to obtain recirculation zones at higher values of stagnation pressure ratio. On the other hand, as the Mach number was increased the value of stagnation pressure ratio necessary to observe a recirculation diminished.

6. ACKNOWLEDGEMENTS

The authors gratefully acknowledge the support for the present research provided by Conselho Nacional de Desenvolvimento Científico e Tecnológico, CNPq, under the Research Grants No. 309985/2013-7, No. 400844/2014-1, No. 443839/2014-0 and 403904/2016-1. The work is also supported by Fundação de Amparo à Pesquisa do Estado de São Paulo, FAPESP, under Research Grant No. 2013/07375-0. The support provided by Fundação Coordenação de Aperfeiçoamento de Pessoal de Nível Superior, CAPES, through graduate scholarship for the first author is also greatly appreciated. This work was performed while L. F. Figueira da Silva was on leave from Institut Pprime, CNRS, France.

7. REFERENCES

Cattafesta III, L.N. and Settles, G.S., 2001. "Experiments on Shock/Vortex Interactions". In *30th Aerospace Sciences Meeting and Exhibit*. AIAA Paper No. 92-0315, Reno, Nevada.

Figueira da Silva, L.F., Sabel'nikov, V. and Deshaies, B., 1997. "Stabilization of Supersonic Combustion by a Free Recirculating Bubble: A Numerical Study". *AIAA Journal*, Vol. 35, No. 11, pp. 1782–1784.

Gruber, M.R., Donbar, J.M., Carter, C.D. and Hsu, K.Y., 2004. "Mixing and Combustion Studies Using Cavity-Based Flameholders in a Supersonic Flow". *AIAA Journal*, Vol. 20, No. 5, pp. 769–778.

Harten, A., 1983. "High Resolution Schemes for Hyperbolic Conservation Laws". *Journal of Computational Physics*, Vol. 49, pp. 357–393.

Harten, A., 1984. "On a Class of High Resolution Total-Variation-Stable Finite-Difference Schemes". *SIAM Journal of Numerical Analysis*, Vol. 21, pp. 1–23.

Kalkhoran, I.M., 1994. "Vortex Distortion During Vortex-Surface Interaction in a Mach 3 Stream". *AIAA Journal*, Vol. 32,

No. 1, pp. 123–129.

Kalkhoran, I.M., Smart, M.K. and Betti, A., 1996. "Interaction of Supersonic Wing-tip Vortices With a Normal Shock". *AIAA Journal*, Vol. 34, No. 9, pp. 1855–1861.

Klass, M., Thomer, O. and Schroder, W., 2002. "Experimental and Computational Investigation of Oblique Shock-Vortex Interaction". In *32nd AIAA Fluid Dynamics Conference and Exhibit*. AIAA Paper No. 2002-3305, St. Louis, Missouri.

Kundu, P., Cohen, I. and Dowling, D., 2015. *Fluid Mechanics*. Elsevier Science.

LeVeque, R., 2002. *Finite Volume Methods for Hyperbolic Problems*. Cambridge Texts in Applied Mathematics. Cambridge University Press.

Mahesh, K., 1996. "A Model for the Onset of Breakdown in an Axisymmetric Compressible Vortex". *Physics of Fluids*, Vol. 8, No. 12, pp. 3338–3345.

Matunaga, M.A.L., 2018. *Onset of Recirculation Bubbles in Inviscid Supersonic Flows*. Master Thesis, Instituto Tecnológico de Aeronáutica, São José dos Campos, SP, Brazil.

Metwally, O., Settles, G. and Hortsman, C., 1989. "An Experimental Study of Shock Wave/Vortex Interaction". In *27th AIAA Aerospace Sciences Meeting*. AIAA Paper No. 89-0082, Reno, NV.

Mitani, T. and Kouchi, T., 2005. "Flame Structures and Combustion Efficiency Computed for a Mach 6 Scramjet Engine". *Combustion and Flame*, Vol. 142, No. 3, pp. 187–196.

Nedungadi, A. and Lewis, M.J., 1996. "Computational Study of the Flowfields Associated with Oblique Shock/Vortex Interactions". *AIAA Journal*, Vol. 34, No. 12, pp. 2545–2553.

Rizetta, D.P., 1997. "Numerical Simulation of Vortex-Induced Oblique Shock-Wave Distortion". *AIAA Journal*, Vol. 35, No. 1, pp. 209–211.

Roe, P.L., 1981. "Approximate Riemann Solvers, Parameter Vectors, and Difference Schemes". *Journal of Computational Physics*, Vol. 43, No. 2, pp. 357 – 372.

Roe, P.L., 1986. "Characteristic-Based Schemes for the Euler Equations". *Annual Review of Fluid Mechanics*, Vol. 18, No. 1, pp. 337–365.

Smart, M.K. and Kalkhoran, I.M., 1995. "Effect of Shock Strength on Oblique Shock-Wave/Vortex Interaction". *AIAA Journal*, Vol. 33, No. 11, pp. 2137–2143.

Thakur, A. and Segal, C., 2008. "Concentration Distribution in a Supersonic Flow Recirculation Region". *Journal of Propulsion and Power*, Vol. 24, No. 1, pp. 64–73.

Toro, E.F., 1997. *Riemann Solvers and Numerical Methods for Fluid Dynamics*. Springer-Verlag Berlin Heidelberg, Berlin, 3rd edition.

Versteeg, H.K. and Malalasekera, W., 2007. *An Introduction to Computational Fluid Dynamics: The Finite Volume Method*. Prentice Hall, Harlow.

Winterfeld, G., 1968. "On the Burning Limits of Flame-Holder-Stabilized Flames in Supersonic Flows". *Advanced Components for Turbojet Engines*, Vol. AGARD CP-34, No. Pt. 1 Paper 28, p. 12.

Yee, H.C., Warming, R.F. and Harten, A., 1982. "A High-Resolution Numerical Technique for Inviscid Gas-Dynamic Problems with Weak Solutions". *Proceedings of the 8th International Conference on Numerical Methods in Fluid Dynamics*, Vol. 170, No. 3, pp. 546–552.

Yee, H.C., Warming, R.F. and Harten, A., 1985. "Implicit Total Variation Diminishing (TVD) Schemes for Steady-State Calculations". *Journal of Computational Physics*, Vol. 57, No. 3, pp. 327–360.

8. RESPONSIBILITY NOTICE

The authors are solely responsible for the printed material included in this paper.